Improved AFEM algorithm for bioluminescence tomography based on dual-mesh alternation strategy

Wei Li (李 维), Heng Zhao (赵 恒), Xiaochao Qu (屈晓超), Yanbin Hou (侯彦宾), Xueli Chen (陈雪利), Duofang Chen (陈多芳), Xiaowei He (贺小伟), Qitan Zhang (张岐坦), and Jimin Liang (梁继民)*

Life Sciences Research Center, School of Life Sciences and Technology, Xidian University, Xi'an 710071, China

**Corresponding author: jimleung@mail.xidian.edu.cn*

Received April 19, 2011; accepted August 3, 2011; posted online September 30, 2011

Adaptive finite element method (AFEM) is broadly adopted to recover the internal source in biological tissues. In this letter, a novel dual-mesh alternation strategy (dual-mesh AFEM) is developed for bioluminescence tomography. By comprehensively considering the error estimation of the finite element method solution on each mesh, two different adaptive strategies based on the error indicator of the reconstructed source and the photon flux density are used alternately in the process. Combined with the constantly adjusted permissible region in the adaptive process, the new algorithm can achieve a more accurate source location compared with the AFEM in the previous experiments.

OCIS codes: 170.6960, 170.3010.

doi: 10.3788/COL201210.021701.

Bioluminescence tomography (BLT), as a molecular imaging modality, has attracted considerable attention for the study of biological processes *in vivo* at the cellular and molecular levels. Moreover, it is a potential technique for cancer detection, drug discovery, and gene expression visualization[1,2]. The major advantages of BLT are sensitivity, low cost, ease of operation, and low noise (in contrast to fluorescence imaging). BLT also allows localization and quantification of internal biological sources generated by the luminescent enzyme and luciferase, which may reveal various molecular and cellular activities in three dimensions[3].

The source reconstruction algorithm has remained a challenging task due to the ill-posedness of the inverse problem in theory. Hence, sufficient *a priori* information including optical parameters, anatomical structure, and permissible source region have tremendous effect on the algorithm[3−6]. In addressing the irregular heterogeneous region, the finite element method (FEM), a classical technique has been widely used, particularly in the inverse problem[7−9]. Accurate numerical solutions require fine discretizations of the tissue volume and large computational resources. Adaptive FEM (AFEM) can achieve a relatively accurate result with low computation cost. In the adaptive process, the strategies of mesh refinement indicated by the error estimation are the core issue. These strategies have significant effect on the precision of the reconstruction result.

In previous studies, Lv *et al.* proposed a multilevel AFEM method which employed two different *a posteriori* error estimations in the forbidden and permissible source regions on the same mesh[10]. Han *et al.* developed an hp-FEM for BLT using linear or quadratic interpolation basis functions for selected elements[11]. In this letter, a novel AFEM for BLT was extended. Both the discrete error estimation of the source and the flux density on the whole mesh were considered comprehensively. Consequently, both the direct maximum selection method and Kelly's error estimation of flux density were utilized as indicators. Subsequently, the mesh refinement was carried out alternately according to the two indicators on the two meshes to avoid overly detailed refinement which could aggravate the ill-posedness of the problem[12]. Furthermore, in the adaptive process, hp-refinement was chosen for the selected elements on a certain mesh, incorporating the constantly adjusted source permissible region in the adaptive process. As such, more accurate and stable results were obtained. Actual mouse experiments demonstrated the advantage of our new algorithm.

In bioluminescence imaging experiments, the bioluminescent photon scattering predominates over absorption in biological tissues, and the photon transport can be described by the diffusion equation[5,10]. The goal of BLT is to obtain the reconstruction of the internal source from the measurement of the emission of light on the surface. Using FEM and the classical Tikhonov regularization method[6], we can express the solution of BLT as

$$\min_{S_{\inf}\leqslant S^{\rm per}\leqslant S_{\sup}} \Theta(S^{\rm per}) = \|\mathbf{A}S^{\rm per} - \Phi^{\rm b}\|_{L^2(\partial\Omega)} + \lambda\|S^{\rm per}\|_{L^2(\Omega)}, \quad (1)$$

where $\Theta(S^{\rm per})$ is the objective function, $S_{\inf}$ and $S_{\sup}$ are the lower and upper bounds of the source density $S^{\rm per}(\mathrm{W/mm^3})$, Ω is the solving domain, $\mathbf{A}$ is the system matrix, $\Phi^{\rm b}$ is the measured flux density on the boundary $\partial\Omega$, and λ denotes the regularization parameter which is manually optimized in this letter.

Considering the approximation $\Phi^{\rm h}(S^{\rm h})$ and $S^{\rm h}$ to the exact solution $\Phi(S)$ and the uniqueness solution of the BLT problem S, the error bound is derived as[13]

$$\|\Phi(S) - \Phi^h(S^h)\|^2_{L^2(\partial\Omega)} + \sqrt{\lambda}\|S - S^h\|^2_{L^2(\Omega)} \leqslant ch^{3/4}. \quad (2)$$

In the AFEM framework, hp-refinement is used for the mesh because hp-refinement can achieve a higher convergence rate compared with h-refinement. Thus, for a tetrahedral element in three dimensions, we have[14]

$$\|\Phi(S) - \Phi^h(S^h)\|_{L^2(\partial\Omega)} \leqslant c'h^p p^{-(t-1/2)}\|\Phi(S)\|_{L^2(\Omega)}. \quad (3)$$

Incorporating Eq. (2) with Eq. (3), the convergence

rate can be expressed as

$$\|\Phi(S) - \Phi^h(S^h)\|^2_{L^2(\partial\Omega)} + 1/2\sqrt{\lambda}\|S - S^{\mathrm{h}}\|^2_{L^2(\Omega)} \leqslant c''h^{2p}p^{-(2t-1)}\|\Phi(S)\|^2_{L^2(\Omega)} + c'''h^{3/4}. \quad (4)$$

In Eqs. (2)–(4), c, c', c'', and c''' are constants which are independent of mesh size h and the order of the interpolation basis functions p, and parameter t depends on the regularity of the exact solution. This illustrates that the BLT solution can be improved by both reducing h and increasing p of the interpolation basis functions. The left side of Eq. (4) indicates that the flux density and the source distribution can determine simultaneously the error bound of the solution on one mesh.

Error estimation plays an important role in AFEM[10]; it indicates whether or not the element on the mesh needs refinement. In the adaptive process, the elements are selected based on both the direct maximum selection method and the *a posteriori* error estimation. The simultaneous use of the two indicators on the same mesh may lead to the intersection problem, which is difficult to handle. Furthermore, the mesh obtained by the adaptive method may be too fine to compute effectively. Therefore, the two types of refinement are operated alternately on the two sequence meshes to avoid an overly detailed mesh which may aggravate the ill-posedness of the problem and increase the computation cost. If the kth level mesh Δ_s^k is considered, it is refined by using *a posteriori* error estimates on the spatial variation of Φ as a first step toward generating a new mesh Δ_Φ^k. For the *a posteriori* error estimation, the Kelly's flux jump criterion $e^\tau(\Phi)$ is used as an error indicator[12]

$$e^\tau(\Phi) = h \oint_{\partial\tau} |\partial\Phi/\partial n|\mathrm{d}a, \quad (5)$$

where $\partial\Phi/\partial n$ is the directional derivative along the normal vector n of the triangular facets of the element τ. In this letter, any element τ on the mesh Δ_s^k is chosen for refinement on the corresponding mesh if

$$e^\tau(\Phi) > \delta_\Phi \max(e^{\Delta_s^k}), \quad (6)$$

where δ_Φ is a constant $(0 < \delta_\Phi < 1)$, and $\max(e^{\Delta_s^k})$ is the maximum value of $e^\tau(\Phi)$ on the mesh. After refinement according to the *a posteriori* indicator, the mesh Δ_Φ^k is obtained for the computation. Thus, there are two meshes at each level, Δ_s^k and Δ_Φ^k, and the mesh Δ_Φ^k is inclined to have a more accurate flux density. The point value from mesh Δ_Φ^k to mesh Δ_s^k is updated based on the solution and the elements for the second refinement are chosen based on mesh Δ_s^k. The new level mesh Δ_s^{k+1} is formed if

$$s^\tau > \beta \max(s^{\Delta_s^k}), \quad (7)$$

where s^τ denotes the density of the tetrahedral element τ in the *a priori* permissible source region, β is a constant $(0 < \beta < 1)$, and $\max(s^{\Delta_s^k})$ is the maximum of s^τ on mesh Δ_s^k. Let the order of the interpolation basis functions be $p = 2$,where p-refinement is performed on the selected tetrahedral element called the quadratic element, and h-refinement is used for the other tetrahedral elements. When the mesh is updated, the quadratic element can be divided into eight linear sub-elements[11].

The initial permissible source region is artificially given as *a priori* knowledge. This may not be accurate and thus, needs to be adjusted. The elements near the source location with higher values of the optimization results most likely represent the actual source. Therefore, the permissible region is revised on each mesh level based on the reconstructed source location and density on the previous mesh level if

$$s_{P_i^j} \geqslant \gamma \max(s) \text{ and } d_{P_i^j} \leqslant \rho, \quad (8)$$

where $s_{P_i^j}$ denotes the density on the ith vertex of the j^{th} element in the permissible region P, γ is a constant $(0 < \gamma < 1)$, $\max(s)$ represents the maximum density of the reconstructed source, $d_{P_i^j}$ is the closest distance from the reconstructed source with higher density to the vertex P_i^j, and $\rho(0 < \rho)$ is the threshold. In other words, the source that is far from the source with large value is not considered as the actual one. This permissible source region strategy may decrease the number of unknowns, thus decreasing the ill-posedness of the BLT problem. The adaptive process can be terminated when the level number reaches its limit $L_{\max}$ or the $\Theta(S^{\mathrm{per}})$ of Eq. (1) attains the minimum value.

In the actual experiment, a heterogeneous mouse was adopted as an object to evaluate the performance of the presented algorithm. All animal procedures were in accordance with the Fourth Military Medical University approved animal protocol. Using the charge-coupled device (CCD) camera and the micro-CT imaging system[15], the anatomical structure and the measured surface data for reconstruction were acquired. Firstly, a luminescent catheter made from a luminescent light stick (Glow Products, Canada) was employed to simulate the bioluminescence source. Subsequently, it was sewn into the abdomen of the mouse. The luminescent catheter emitted luminescent light with a peak wavelength of approximately 640 nm. The corresponding optical parameters shown in Table 1 were calculated based on Ref. [5]. Secondly, the anatomical information of the living mouse and the internal source were obtained by segmenting the micro-CT slices. Subsequently, the relevant optical parameters were assigned to the different organs, such as adipose, heart, lungs, liver, and kidneys. The source information from the micro-CT images was only used to validate the result of the proposed method. The two-dimensional (2D) multi-view overlay images of the photographs and luminescent images were acquired by a CCD camera. To avoid external disturbance, the mouse experiment was performed in a darkroom. Thirdly, the optical data and the volume data of the micro-CT were combined using the methods in Ref. [15].

In the numerical experiment, the same phantom available in Ref. [11] was employed to derive the comparison

Table 1. Optical Parameters of the Mouse Organ Regions

Materials	Muscle	Heart	Lungs	Liver	Kidneys
$\mu_{\mathrm{a}}(\mathrm{mm}^{-1})$	0.009	0.138	0.460	0.829	0.155
$\mu'_{\mathrm{s}}(\mathrm{mm}^{-1})$	1.258	1.077	2.265	0.736	2.533

between hp-FEM and dual-mesh AFEM. With different sizes of the initial mesh, ranging from $h = 1.2$ to 1.7, h is determined as the maximum size of the element in the mesh. Considering the first level reconstruction, the six-group results were obtained using hp-FEM and dual-mesh hp-FEM. Defining the distance error $d = \|x - x_0\|_2$, where x is the reconstructed source center, x and x_0 can be determined as

$$\sum_{\text{elem}} \bar{S}^* \text{Vol}^* \text{Cor} / \sum_{\text{elem},\bar{S}\neq 0} \text{Cor}, \tag{9}$$

where $\bar{S}$ denotes the mean density of the element which varies with x or x_0, Vol is the volume of the element, and Cor is the coordinate of the tetrahedron element center.

The different mesh may result in different interpolate errors. This may lead to the inaccuracy of the source intensity. Thus, the source location error was obtained, as shown in Fig. 1. However, it is clear that the location results obtained by our method are stable under the error of 0.55 mm, whereas the result of hp-FEM has a wide fluctuation when the mesh size varies.

Mouse experiment was also carried out to compare the previous hp-FEM and the dual-mesh AFEM algorithms. After acquiring the dual modality data, the data gained from the CCD camera were mapped onto the surface of the mouse using the surface flux reconstruction method[16], as shown in Figs. 2 and 3. Using the volume data of the micro-CT, the mouse was discretized into 21019 elements and 3975 nodes for the FEM calculation. Two initial permissible source regions of different sizes were adopted to reconstruct the source. The smaller Ω_S was set as $\{(x, y, z)|14 < x < 19, 15 < y < 20, 7 < z < 12\}$, and the larger Ω_L was set as $\{(x, y, z)|13 < x < 21, 13 < y < 22, 6 < z < 13\}$. The actual source center x_0 was localized at (15.7, 17.6, 11.2).

The results of computations using the two algorithms are shown in Table 2, Figs. 4 and 5. For the hp-FEM algorithm, the distance between the reconstructed source center and actual center is 1.78 mm, which worsened when the permissible regions are larger (d=2.22 mm). On the contrary, the source location center obtained using the dual-mesh AFEM algorithm is much closer to the real one, with errors of 0.93 and 1.63 mm for the two cases. The BLT reconstruction program was coded by MATLAB in a desktop computer (Intel(R) Core(TM) 2 Quad CPU Q8400 @ 2.66 GHz and 3.49G RAM). The time cost of the two algorithms is approximately 160 s.

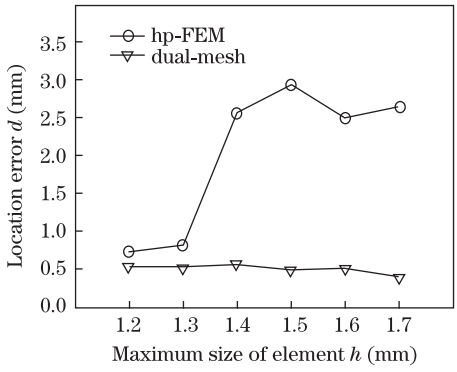

Fig. 1. Relationship between the source location error d and initial meshes of different sizes of h.

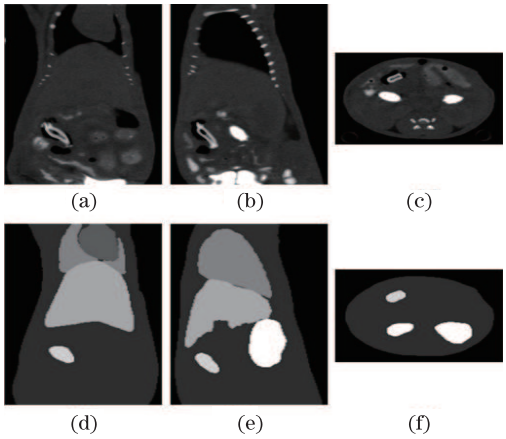

Fig. 2. (a)–(c) Micro-CT slices of the mouse, (d)–(f) segmentation of the volume in muscle, heart, lungs, liver, kidneys, and the source for the same slices.

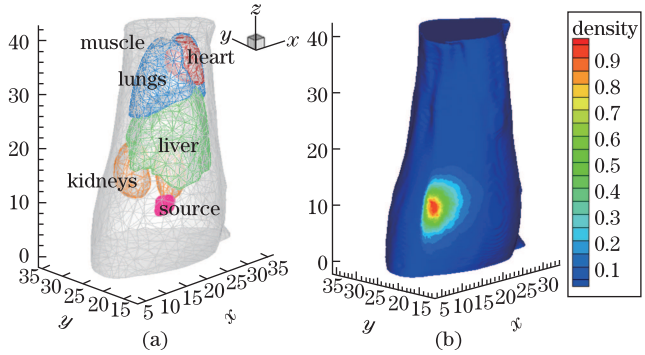

Fig. 3. (a) Heterogeneous mouse mesh for the actual experiment and actual source location acquired by CT data segmentation; (b) photo flux density on the surface of the mouse after mapping from 2D data obtained by the CCD camera.

Error estimation is a significant indicator for element mesh refinement. Considering the error estimation for both the source and flux density comprehensively, a novel dual-mesh AFEM algorithm was proposed. The two refinements used in the algorithm were carried out alternately based on the different error estimations (10, 11). The actual experiment indicates that more accurate

Table 2. Reconstruction Results of the Heterogeneous Mouse Experiment

Permissible Source Region	Algorithm	Reconstructed Location	d (mm)	Time Cost (s)
Ω_S	hp-FEM	(14.95, 19.01, 10.37)	1.78	157.93
	Dual-mesh AFEM	(14.86, 17.15, 11.23)	0.93	168.80
Ω_L	hp-FEM	(13.87, 18.31, 12.27)	2.22	165.25
	Dual-mesh AFEM	(14.74, 17.93, 12.49)	1.63	169.03

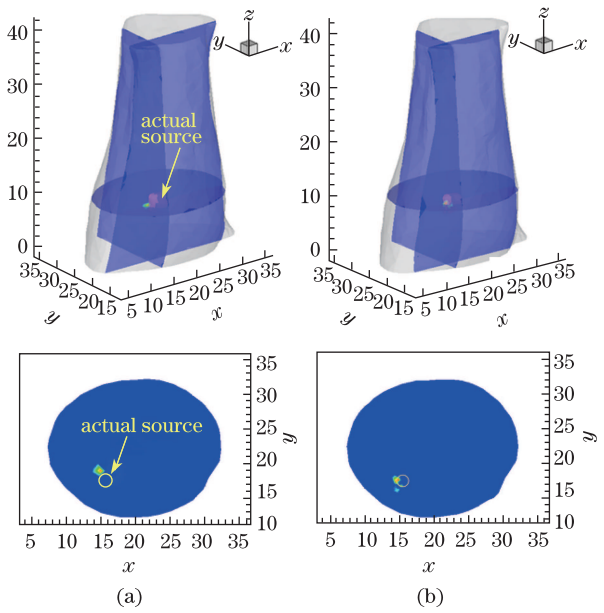

Fig. 4. Reconstruction results of source location with a smaller permissible region Ω_S using (a) hp-FEM and (b) dual-mesh AFEM.

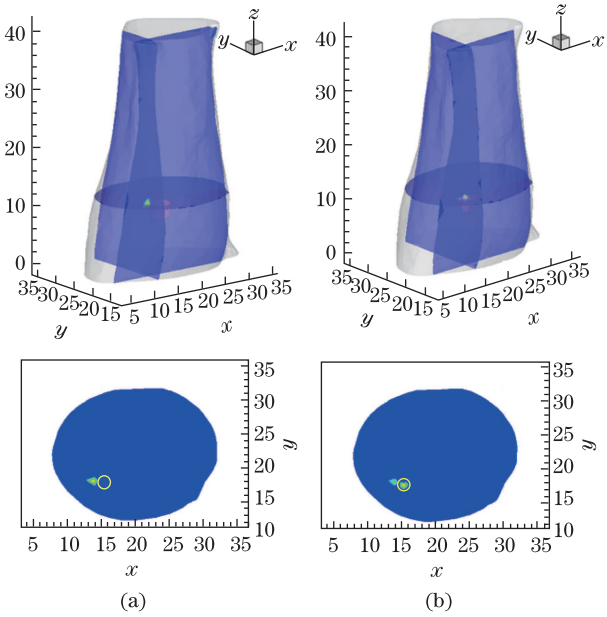

Fig. 5. Reconstruction results of the source location with a larger permissible region Ω_L using (a) hp-FEM and (b) dual-mesh AFEM.

and stable location results are achieved by our algorithm compared with the previous adaptive FEM method.

For BLT reconstruction, the permissible source region, as *a priori* information, plays an important role in improving the ill-posedness of the inverse problem. Thus, the permissible region was gradually adjusted during the adaptive process of our algorithm according to the reconstructed source. The mouse experiment demonstrates the effectiveness of the algorithm. However, the initial permissible source region, as *a priori* information, was still needed. The initial permissible source region selection method or the algorithm without an initial permissible source region needs further investigation.

Reconstructing the source distribution in both location and density is crucial in optical tomography. Numerous factors, including the intrinsic ill-posedness of the problem, optimization method, and photon propagation model, may influence the source reconstruction. Determining the proper method and its optimal parameters, such as the regularization parameter, is valuable for the resolution of this problem. Our future work will focus on the quantitative reconstruction algorithm without the initial permissible source region along with the highly accurate forward models.

This work was supported by the National "973" Program of China (No. 2011CB707702), the National Natural Science Foundation of China (Nos. 81090272, 81000632, and 30900334), the Shaanxi Provincial Natural Science Foundation Research Project (No. 2009JQ8018), and the Fundamental Research Funds for the Central Universities.

References

1. R. Weissleder and M. J. Pittet, Nature **452,** 580 (2008).
2. J. Tian, J. Bai, X.-P. Yan, S. Bao, Y. Li, W. Liang, and X. Yang, IEEE Eng. Med. Biol. Mag. **27,** 48 (2008).
3. G. Wang, Y. Li, and M. Jiang, Med. Phys. **31,** 2289 (2004).
4. J. Feng, K. Jia, C. Qin, S. Zhu, X. Yang, and J. Tian, Chin. Opt. Lett. **8,** 1010 (2010).
5. G. Alexandrakis, F. R. Rannou, and A. F. Chatziioannou, Phys. Med. Biol. **50,** 4225 (2005).
6. W. Cong, G. Wang, D. Kumar, Y. Liu, M. Jiang, L. V. Wang, E. A. Hoffman, G. McLennan, P. B. McCray, J. Zabner, and A. Cong, Opt. Express **13,** 6756 (2005).
7. D. Wang, X. Liu, Y. Chen, and J. Bai, Chin. Opt. Lett. **8,** 82 (2010).
8. X. Song, D. Wang, N. Chen, J. Bai, and H. Wang, Opt. Express **15,** 18300 (2007).
9. P. Ruan, F. Gao, F. Yang, and H. Zhao, Chin. Opt. Lett. **8,** 787 (2010).
10. Y. Lv, J. Tian, W. Cong, G. Wang, J. Luo, W. Yang, and H. Li, Opt. Express **14,** 8211 (2006).
11. R. Han, J. Liang, X. Qu, Y. Hou, N. Ren, J. Mao, and J. Tian, Opt. Express **17,** 14481 (2009).
12. D. W. Kelly, J. P. De, S. R. Gago, O. C. Zienkiewicz, and I. Babuska, Int. J. Numer. Meth. Eng. **19,** 1593 (1983).
13. G. Wang, W. Cong, Y. Li, W. Han, D. Kumar, X. Qian, H. Shen, M. Jiang, T. Zhou, J. Cheng, J. Tian, Y. Lv, H. Li, and J. Luo, in *Proceedings of the Third IEEE International Symposium on Biomedical Imaging* 678 (2006).
14. M. Ainsworth and B. Senior, Comput. Meth. Appl. Mech. Eng. **150,** 65 (1997).
15. J. Liu, Y. Wang, X. Qu, X. Li, X. Ma, R. Han, Z. Hu, X. Chen, D. Sun, R. Zhang, D. Chen, D. Chen, X. Chen, J. Liang, F. Cao, and J. Tian, Opt. Express **18,** 13102 (2010).
16. X. Chen, X. Gao, D. Chen, X. Ma, X. Zhao, M. Shen, X. Li, X. Qu, J. Liang, J. Ripoll, and J. Tian, Opt. Express **18,** 19876 (2010).